Available online at BCREC website: https://bcrec.id

Bulletin of Chemical Reaction Engineering & Catalysis, 17 (2) 2022, 340-349

Research Article

Hydrothermal Synthesis and Photocatalytic Activity of NiO Nanoparticles under Visible Light Illumination

J. Anita Lett[1], Suresh Sagadevan[2,*], Getu Kassegn Weldegebrieal[3], Is Fatimah[4,*]

[1]Department of Physics, Sathyabama Institute of Science and Technology, Chennai, Tamil Nadu, India.
[2]Nanotechnology & Catalysis Research Centre, University of Malaya, Kuala Lumpur 50603, Malaysia.
[3]Department Chemistry, College of Natural and Computational Sciences, Debre Berhan University, Ethiopia.
[4]Department of Chemistry, Faculty of Mathematics and Natural Sciences, Universitas Islam Indonesia, Kampus Terpadu UII, Jl. Kaliurang Km 14, Sleman, Yogyakarta, Indonesia.

Received: 17th February 2022; Revised: 11th April 2022; Accepted: 11th April 2022
Available online: 14th April 2022; Published regularly: June 2022

Abstract

In this present study, Nickel oxide (NiO) nanoparticles (NPs) have been synthesized using the hydrothermal method and characterized using powder X-ray Diffraction (XRD), UV-vis and Fourier Transform Infra Red (FTIR) spectroscopies, Scanning Electron Microscopy (SEM), and Energy-Dispersive X-ray (EDX) methods. The result of the characterization indicates that the synthesized sample has a pure cubic phase of NiO with roughly spherical shape morphologies and respective estimated crystallinity and microstrain values of about 78% and 5.1. Test of the photocatalytic activity of the synthesized sample towards the model contaminant dye methylene blue (MB) shows a degradation efficiency of 46% in a period of 2 h under nature sunlight irradiation at natural pH and that the reaction could satisfactorily describe both pseudo-first-order and pseudo-second-order kinetic models. So, this synthesis method may potentially be used for the effective elimination of toxic organic pollutants from water and wastewater over prolonged exposure under natural sunlight without adding any oxidant or adjusting the pH of the reaction medium.

Keywords: Nickel oxide; Nanoparticles; Hydrothermal synthesis; Optical properties; Photocatalytic activity

How to Cite: J. Anita Lett, S. Sagadevan, G.K. Weldegebrieal, I. Fatimah (2022). Hydrothermal Synthesis and Photocatalytic Activity of NiO Nanoparticles under Visible Light Illumination. *Bulletin of Chemical Reaction Engineering & Catalysis*, 17(2), 340-349 (doi: 10.9767/bcrec.17.2.13680.340-349)

Permalink/DOI: https://doi.org/10.9767/bcrec.17.2.13680.340-349

1. Introduction

Environmental pollution is the most serious problem facing in the world today, with scientists recommending that conditions be created to achieve a clean and healthy environment for a better life in the world [1–3]. Population and global production growth have been linked to a dramatic increase in the use of chemicals in recent decades, due to their daily entry into the environment and resistance to biodegradation, which may result in the generation of hazards for various species [4–7]. To prevent water and environmental pollution caused by the arrival of polluted industrial effluents, appropriate strategies for their treatment and reuse must be developed [8,9]. Today, safe and hygienic drinking water is a unique requirement of the global health community [10,12]. The critical feature of

* Corresponding Authors.
Email: drsureshnano@gmail.com (S. Sagadevan);
isfatimah@uii.ac.id (I. Fatimah);

densely populated and industrial areas close to water resources has resulted in the assumption of difficult global issues [13,14]. Designing novel wastewater treatment methods while taking into account their shortcomings leads to an increase in their ability and performance in removing various contaminants from aqueous media [15].

The problem with traditional wastewater treatment methods such as adsorption, chemical oxidation, flotation, flocculation, membrane filtration, adsorption, *etc.* is that they involve physical separation of the pollutants rather than eliminating them, have sludge formation, and are generally cost-ineffective and environmentally unfriendly approaches. Heterogeneous photocatalysis, which utilizes catalysts for catalyzing photochemical reactions, is a promising technique for eliminating pollutants from water and wastewater in a cost-efficient and environmentally friendly manner [16–20].

Nickel oxide (NiO) is one of the semiconductor transition metal oxides having such interesting applications as in the manufacture of photochromic materials, magnets, transparent conducting films, electrochemical capacitors, gas sensors, electrodes in alkaline batteries and solid oxide fuel cells, antibacterial agent, and catalysis [21]. It is a p-type semiconductor oxide with an indirect bulk bandgap of 3.5 eV and exhibits antiferromagnetic and Mott insulator behavior [22], high conductivity, good switching speed, stable and well-defined redox kinetics, *etc.* [23]. Various synthesis methods including sol-gel [24], hydrothermal [25], thermal decomposition [26], microwave irradiation [27], solid-state reaction [28], precipitation, and sonochemical reaction [29], *etc.* have been employed to synthesize NiO nanostructures with different particle size, shape, and dimensionality for application in different sectors.

The photocatalytic degradation efficiency of NiO NPs towards organic pollutants depends on the synthesis method employed while other experimental parameters are kept constant because the different synthesis methods can yield NiO nanostructures with different particle morphologies and crystal structures. For example, The photocatalytic decomposition percentage of methyl orange dye using NiO synthesized by emulsion nanoreactors method was found to be greater than that synthesized by hydrothermal, sol-gel, and thermal decomposition method, as reported by Fazlali *et al.* [30]. According to the authors, the enhanced catalytic activity of NiO structures synthesized by the emulsion nanoreactors method compared to the other approaches was due to the low scattering of light, large surface-active sites, and greater stability in a solvent of the resulting spherical like morphologies relative to plate-like, nanowood, and flower-like shapes produced by the other synthesis methods, respectively. Miri *et al.* [31] reported a degradation efficiency of 65.5% in the methylene blue dye using biosynthesized NiO NPs under UV light irradiation for a period of 3 h.

The solvothermal synthesis method has such advantages as simplicity, high crystallinity of obtained product at a relatively low temperature of about 180 °C, and the ability to control crystal growth while producing a large quantity of products [32]. In this work, NiO nanoparticles are synthesized using the hydrothermal method and its photocatalytic degradation performance is evaluated for the model contaminant dye methylene blue dye using natural sunlight as a source of radiation.

2. Materials and Methods

2.1 Materials

NiO nanostructures were formed by the hydrothermal synthesis route of nickel acetate, $Ni(CH_3COO)_2.2H_2O$ (purchased from Sigma-Aldrich, Mumbai, India). All the chemicals and solvents used during the synthesis are analytic-grade reagents and were used as received without any further purification. Distilled water (DW) was used throughout the experiment.

2.2 Synthesis of NiO Nanoparticles

For the synthesis of NiO NPs, the first 0.5 g of nickel acetate was dissolved in 100 mL of DW. Next, the solution was mixed under constant magnetic stirring to ensure homogeneity. Then, the solution was transferred into a 50 mL capacity Teflon-lined stainless-steel autoclave, sealed and put in an oven whose temperature is maintained at 180 °C for 24 h. Finally, the autoclave was cooled to room temperature and the resulting greenish precipitate formed was washed with DW first (to remove any excess ions), and then with ethanol, dried in an oven at 60 °C for 5 h to obtain the NiO NPs, which has been stored carefully for next characterization and application purpose.

2.3. Photocatalytic Study

We have examined the photocatalytic activity of the formed NiO nanopowder for Methylene blue (MB) dye. Firstly, 40 mg of the catalyst sample was used to degrade 80 mL of 2×10^{-5} M dye concentration for 120 min and aliquot sample solutions were collected at regu-

lar time intervals of 15 min. Before starting the experiment, the sample mixture of catalyst particles and dye solution was stirred at room temperature in the dark condition for 30 min. Then after the exposure of the reaction mixture to sunlight, the absorbance of the aliquots taken at regular time intervals was measured at the maximum wavelength of absorption (665 nm) of the dye with a UV-vis spectrophotometer. The absorption intensity of dyes decreased significantly in the presence of light in comparison with reaction at dark with a photocatalyst, which confirms the effective degradation ability of the sample. The variation in the ratio of the concentration (C) after irradiation to the initial concentration (C_0) as a function of irradiation time with different photocatalysts is also derived and presented. The degradation efficiency (Degradation (%)) of MB dye was calculated with the help of Equation (1),

$$Degradation\ (\%) = \frac{A_0 - A_t}{A_0} \times 100 \quad (1)$$

where, A_0 and A_t are dye absorbance before and after exposure to visible light irradiation, respectively.

2.4 Instrumental Analysis

Powder X-ray diffraction (XRD) analysis was carried out using on Rigaku multiflex diffractometer (Japan) that operates at 3 kW power and uses the Cu-Kα radiation (λ=1.5408 Å and 2θ of 10–80° range). Fourier transform infrared (FTIR) spectroscopic analysis was carried out using on Spectrum 100 FT-IR instrument (Perkin Elmer, USA) and the samples for analysis were prepared using the KBr pellet method (wavenumber range of 4000–400 cm^{-1}). The UV-Vis spectral analysis was performed on a Cary 50 UV-Vis spectrophotometer (Varian technologies, USA). The scanning electron microscopy (SEM) images were taken on the FEI-Quanta FEG 200F instrument (Thermo Fisher Scientific, USA) connected to energy dispersive analysis by X-rays (EDAX) detector.

3. Results and Discussion

3.1. Physicochemical Characterization

NiO NPs formed by the hydrothermal synthesis method is analyzed for crystallinity, crystal sizes, and phase purity using the powder XRD analysis, where the diffraction patterns in the 2θ range of 20–80° are provided in Figure 1. From the spectrum shown, NiO NPs have the reflection patterns along the crystal planes of (111), (200), (220), (311), and (222)

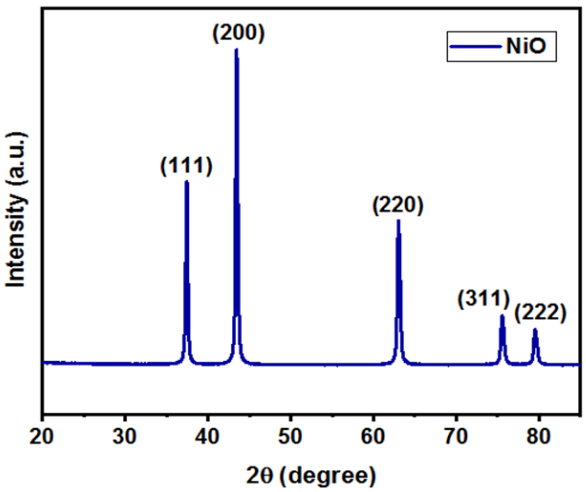

Figure 1. Powder XRD pattern of the synthesized NiO NPs.

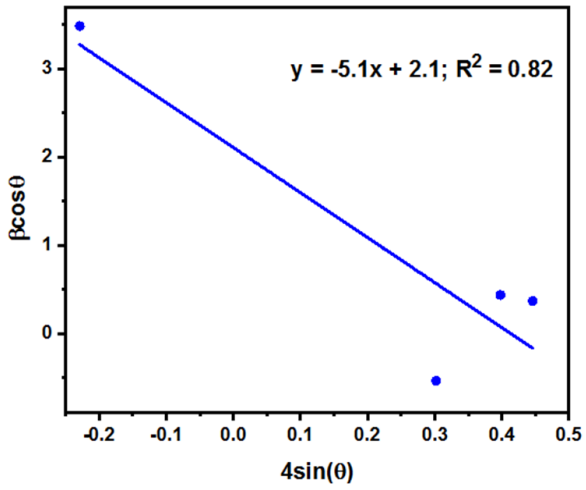

Figure 2. W-H plot for the synthesized NiO nanoparticles.

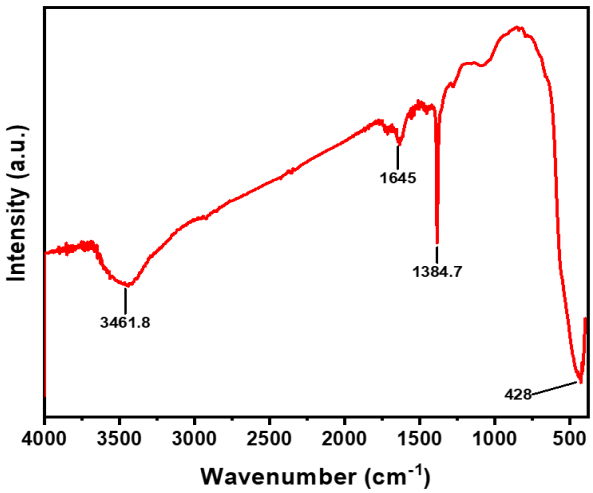

Figure 3. FTIR spectrum of the synthesized NiO NPs.

which can be attributed to the formation of the cubic structure of NiO [21]. Also, as provided in the figure, the diffraction patterns formed are of sharp, narrow, and significant intensity peaks where all these factors support the crystalline nature of the formed NiO. Moreover, the absence of other peaks indicates the phase purity of the obtained NiO product.

The average crystallite size (D) calculated using Scherrer formula, Equation (2) is 24.5 nm.

$$D = \frac{k\lambda}{\beta \cos\theta} \tag{2}$$

where, k = shape factor Scherrer constant value equal to 0.9, λ is the wavelength of the x-ray

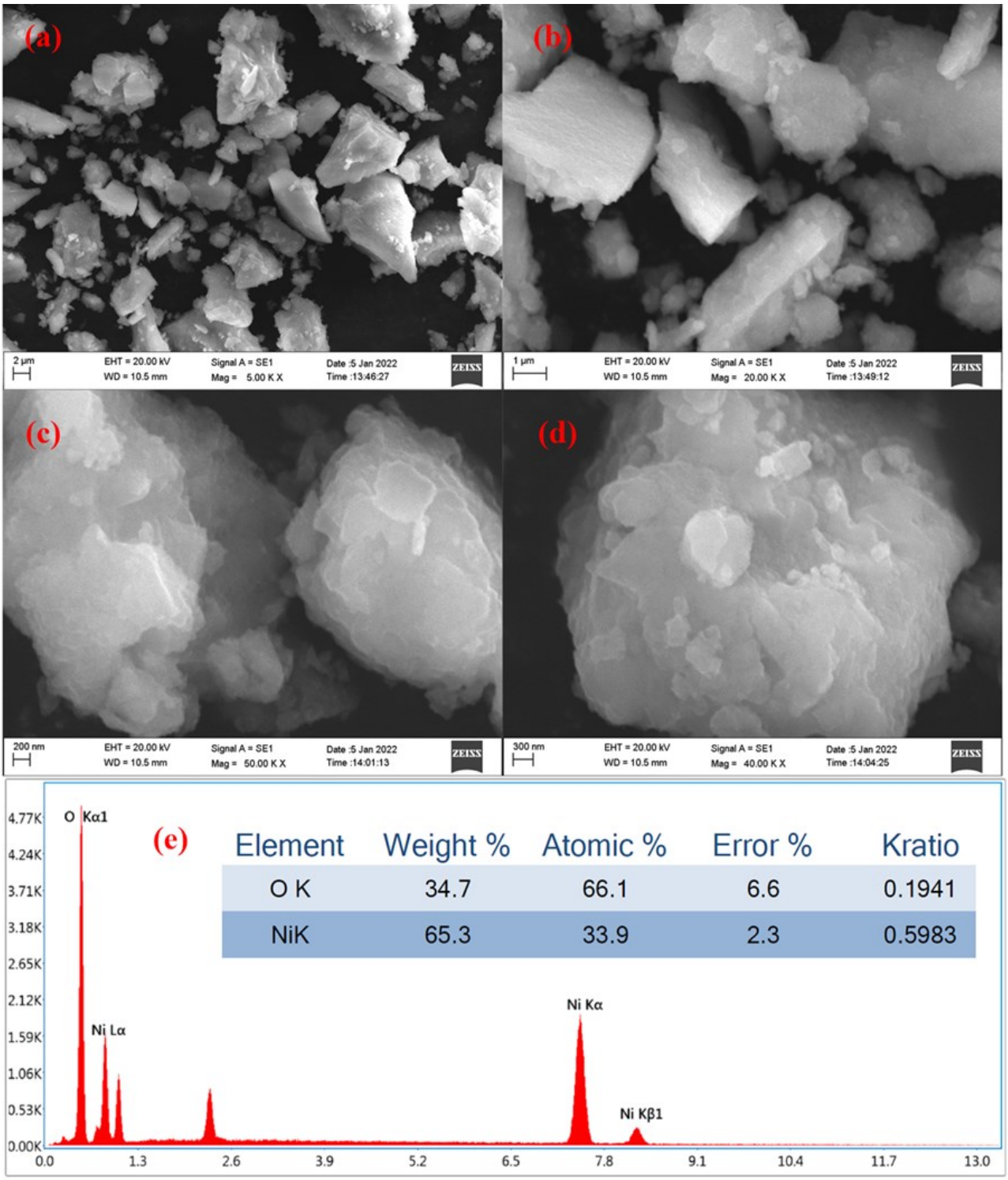

Figure 4. SEM images at different magnifications (a-d) and EDX spectrum (e) of NiO NPs.

radiation source Cu-Kα = 0.15406 nm, β and θ are the peak width at half maximum intensity and Bragg angle, respectively. The crystallinity of the synthesized NiO NPs, calculated using Equation (3) by dividing the area of all crystalline peaks (A_C) to that of the area of all peaks (crystalline plus amorphous, (A_C+A_A)) was 77.84%.

$$Crystallinity\ (\%) = \frac{A_C}{A_C + A_A} \times 100 \quad (3)$$

The microstrain (ε) in the synthesized NiO sample powder obtained from the Williamson-Hall plot method, Figure 2 and applying Equation (4) is about 5.1.

$$\beta \cos\theta = \varepsilon 4 \sin\theta + \frac{k\lambda}{D} \quad (4)$$

Figure 3 provides the FTIR spectral analysis of synthesized NiO NPs. Metal oxides generally give absorption bands below 1000 cm^{-1} arising from inter-atomic vibrations. From the FTIR spectrum, the broad and sharp peaks situated at 3461, 1645, and 1384.7 cm^{-1} can be correlated to the −OH stretching and bending vibrations of adsorbed water molecules; however, the peak observed around 1135 cm^{-1} is indicating the hydroxyl group of surface adsorbed hydrated molecules. From the spectrum, the observation of a band at 428 cm^{-1} is attributed to Ni−O stretching vibration and thereby confirming the formation of the NiO compound.

Figure 4 (a-d) shows the SEM images of as-prepared NiO NPs at different magnifications in and from the figure, there is an aggregation or overlapping of smaller sized NiO particles to generate the larger ones. Also, from the SEM images, the grains seem to be distributed randomly and are maintaining the homogeneous rod-like morphology. Further, the EDAX provided elemental analysis of NiO NPs shown in Figure 4(e) confirmed the presence of Ni and O elements in the powdered sample.

The EDS elemental mapping of the synthesized NiO NPs is shown in Figure 5. From the figure, it can be seen that the Ni and O ele-

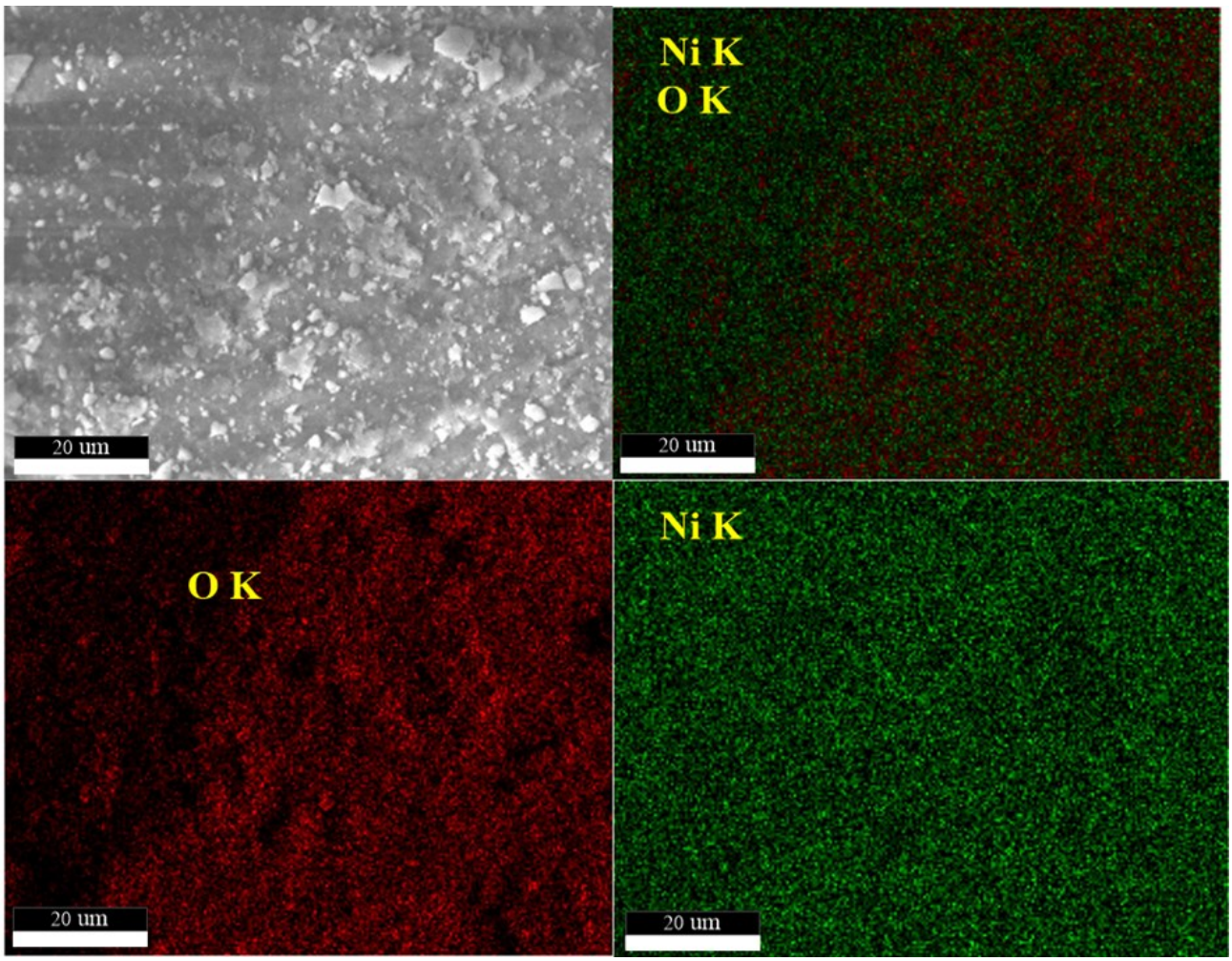

Figure 5. EDS mapping of the synthesized NiO NPs.

ments are evenly distributed confirming the homogeneity of the sample. In addition, the EDAX provided the elemental composition of the NiO sample showed the presence of only two elements (Ni and O), thereby supporting the high purity of the synthesized sample which in turn indicates the efficiency of the hydrothermal synthesis route to produce pure NiO NPs.

The UV-visible absorption spectrum of NiO is depicted in Figure 6(a). The maximum absorption peak at 250 nm of the sample lies in the ultraviolet region. The increasing absorbance broad shoulder of the absorbance peak could be attributed to particle size distribution and defects. The optical bandgap of the NiO NPs was estimated using Tauc's relation, Equation (5).

$$(\alpha h\nu)^2 = A(h\nu - E_g) \quad (5)$$

where, α is the coefficient of absorption, h is Planck's constant, ν is photon energy (eV) and E_g is the bandgap energy in eV. Plotting the $(\alpha h\nu)^2$ versus $h\nu$ as shown in Figure 6(b) and extrapolating the line drawn tangent to the resulting curve gives the value of the bandgap energy. The optical bandgap of the NiO NPs was calculated to be 3.14 eV.

3.2. Photocatalytic Activity Analysis

The photocatalytic performance of the synthesized NiO NPs for the photodegradation of MB dye was studied under sunlight irradiation. As indicated in Figure 7, the absorbance of the sample solutions withdrawn from the reaction mixture went decreasing with time, achieving a degradation performance of 46% in 2 h of irradiation time at natural pH and employing catalyst dose of 40 mg and 80 mL of 0.02 mM dye initial concentration. Negligible decomposition (nearly 12%) was observed in the absence of NiO catalyst but exposure to radiation and no decomposition were noted in a dark room while in the presence of a catalyst sample. This indicates that the observed degradation percentage can be attributed to the photoactivity of the catalyst particles in the reaction medium.

The photodegradation data were fitted with pseudo-first-order and pseudo-second-order reaction models, Equations (6) and (7), respectively and graphically illustrated in Figures 8(a) and (b) and the result exhibited that the data can be described with the specified models

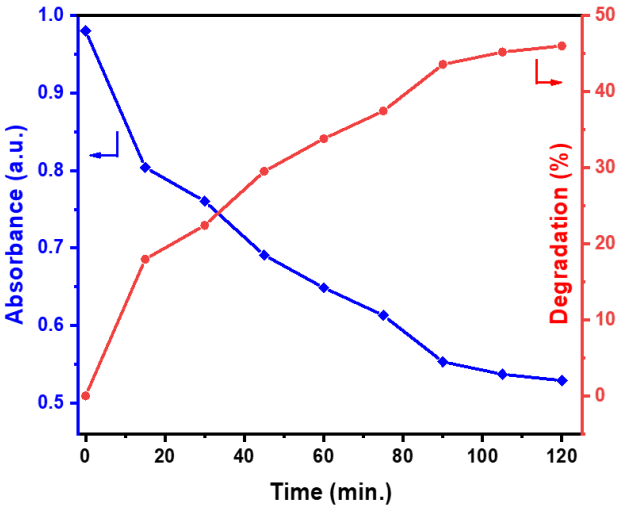

Figure 7. Time-dependent concentration change and degradation were achieved for MB during 2 h of irradiation under visible light

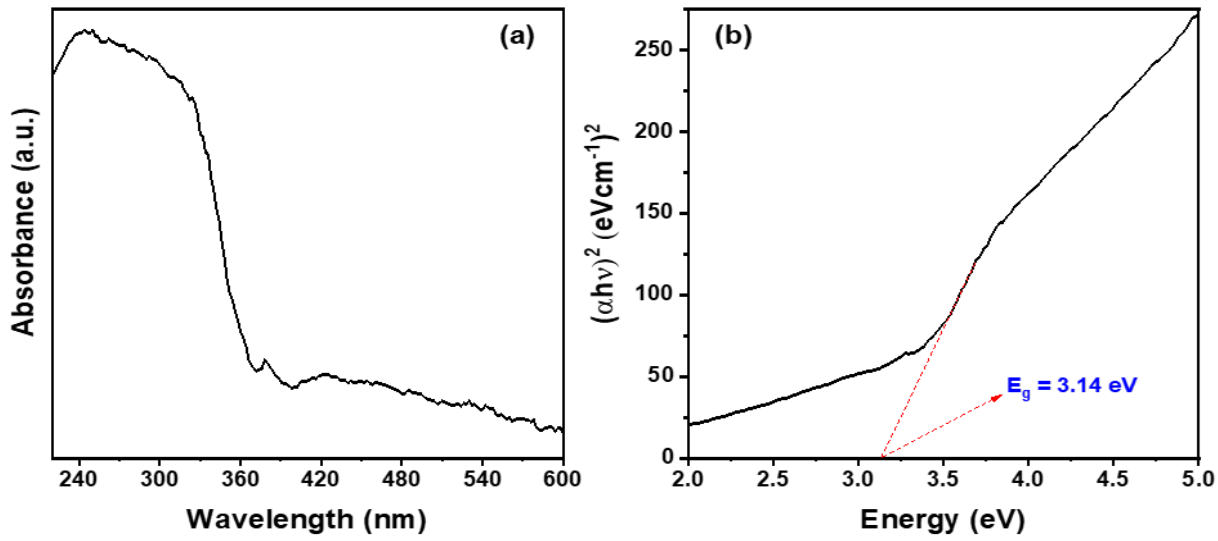

Figure 6. UV-vis absorbance spectrum (a) and the corresponding Tauc's plot (b) of NiO NPs.

with satisfactory values of correlation coefficient (R^2). The half-life of the pseudo-first-order reaction, that is, the reaction time decreases the initial concentration of the dye by half, given by Equation (8) which is 141 min, while that for the second-order reaction is 7×10^7 $min^{-1}.mol^{-1}$, Equation (9) [33]. The kinetics parameters are also summarized in Table 1.

$$\ln\left(\frac{C_0}{C_t}\right) = k_1 t \quad (6)$$

$$\frac{1}{C_t} = \frac{1}{C_0} - k_2 t \quad (7)$$

$$t_{½} = \frac{\ln(2)}{k_1} \quad (8)$$

$$t_{½} = \frac{1}{C_0 k_2} \quad (9)$$

where, k_1, k_2, C_0 and C_t refer to the first order and second-order reaction rate constants, and the initial concentration and concentration after exposure time t, respectively.

3.3 Photocatalytic Degradation Mechanism

Photocatalytic decomposition of organic pollutants using semiconductor photocatalysts may occur through direct or indirect mechanistic routes. In the direct route, degradation occurs by hydroxyl radical (HO•) formed by the direct injection of electrons into the CB of the semiconductor from the photosensitized organic pollutant which results in the reduction of to superoxide radical ion (O_2^{-}•) and then into HO•, Equations (13)–(16). However, in the indirect mechanism of dye degradation into less harmful end products, decomposition occurs following the generation of charge carriers in the semiconductor catalyst surface when radiation of energy greater than or equal to the bandgap energy (E_g) irradiates it and then the subsequent formation of reactive radicals, primarily HO• and O_2^{-}• radicals, Equations (6)–(13) [33,34] and it has been reported that this latter mechanism is a more dominant and kinetically faster route in the photocatalytic degradation of dyes [35].

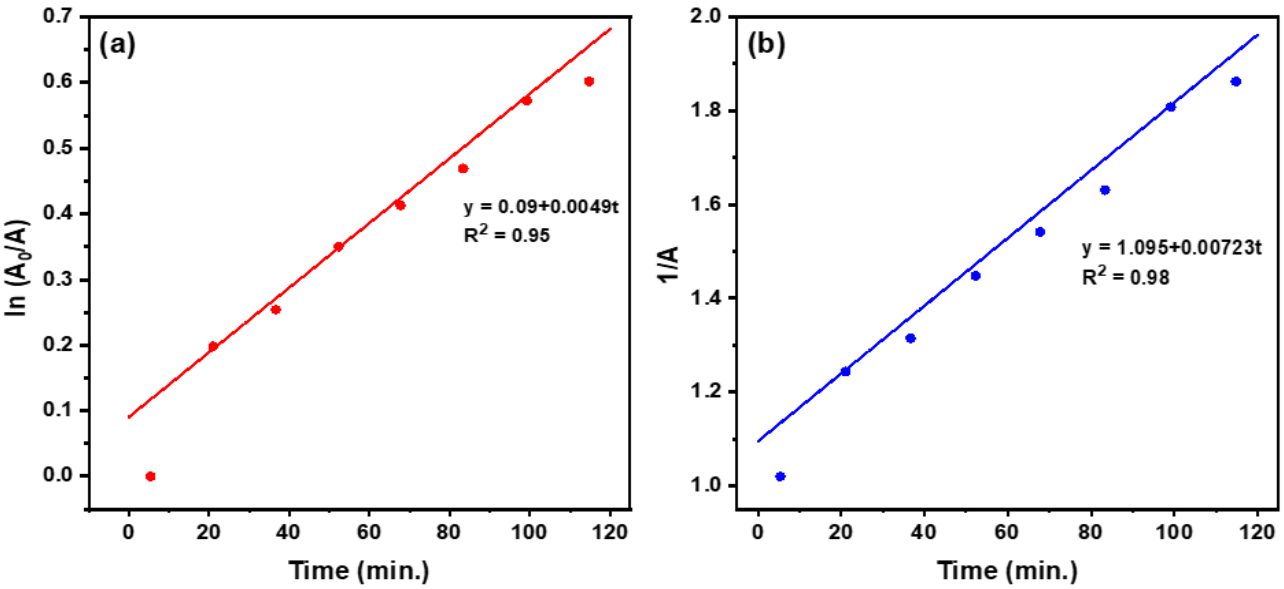

Figure 8. Pseudo-first-order (a) and second-order kinetics (b) plots for the degradation of MB using NiO NPs.

Table 1. Pseudo-first-order and pseudo-second-order reaction kinetics parameters for the degradation of MB dye.

Order of reaction	Reaction rate constant (k_1/k_2)	Degradation (%)	$t_{1/2}$	R^2
Pseudo 1st order	0.0049	46%	141 min	0.95
Pseudo 2nd order	0.00723	46%	7×10^7 $min^{-1}.mol^{-1}$	0.98

$$NiO\ (s) + h\nu \rightarrow NiO\ (s)(e^- + h^+) \quad (10)$$
$$e^- + O_2 \rightarrow O_2^{-\bullet} \quad (11)$$
$$H_2O + h^+ \rightarrow HO^\bullet + H^+ \quad (12)$$
$$MB + h\nu \rightarrow MB^* + O_2 \rightarrow MB^{+\bullet} + O_2^{-\bullet} \quad (13)$$
$$O_2^{-\bullet} + H^+ \rightarrow HOO^\bullet \quad (14)$$
$$2HOO^\bullet \rightarrow H_2O_2 + O_2 \quad (15)$$
$$H_2O_2 \rightarrow 2HO^\bullet \quad (16)$$
$$MB + HO^\bullet/O_2^{-\bullet} \rightarrow \text{Degradation products} \quad (17)$$

4. Conclusion

Nickel oxide is a multifunctional semiconductor oxide used in such application areas as in the manufacture of photochromic materials, magnets, transparent conducting films, electrochemical capacitors, gas sensors, electrodes in alkaline batteries, and solid oxide fuel cells, antibacterial agents, and heterogeneous photocatalysis. Since different synthesis methods employed result in particles with different crystal structures and surface morphologies, the photocatalytic performance could also vary. In this summary, NiO NPs were successfully synthesized using the hydrothermal technique at a relatively lower temperature and characterized thoroughly for their crystallinity, morphology, surface functionality, and optical properties. From the powdered XRD analysis, the as-synthesized NiO was found to be a cubic phase and crystalline nature while the SEM images indicated roughly spherical like particle morphology The FTIR analysis demonstrated evidence for the formation of NiO NPs. The synthesized NiO NPs achieved degradation efficiency of about 46% in 2 h of irradiation under natural sunlight without adjusting the natural pH of the medium. The photodegradation reaction mechanism is mainly attributed to the indirect route and can be described with pseudo-first-order and pseudo-second-order reaction kinetics with a satisfactory value of the correlation coefficient. Therefore, the prepared NiO NPs could potentially be used in the treatment of water or wastewater bearing toxic organic pollutants just by utilizing nature sunlight as a source of radiation.

Acknowledgments

This work was financially supported by University of Malaya Research Grant (RU001-2019, RU001-2020 and RU001-2021).

References

[1] Ghorani-Azam, A., Riahi-Zanjani, B., Balali-Mood, M. (2016). Effects of air pollution on human health and practical measures for prevention in Iran. *Journal of Research on Medical Sciences*. 21 (65). DOI: 10.4103/1735-1995.189646

[2] Manisalidis, I., Stavropoulou, E., Stavropoulos, A., Bezirtzoglou, E. (2020). Environmental and Health Impacts of Air Pollution: A Review. *Front Public Health*. 8 (14). DOI: 10.3389/fpubh.2020.00014

[3] Abdel-Shafy, H.I., Mansour, M.S.M. (2018). Solid waste issue: Sources, composition, disposal, recycling, and valorization, *Egyptian Journal of Petroleum*, 27 (4), 1275-1290. DOI: 10.1016/j.ejpe.2018.07.003

[4] Chamas, A., Moon, H., Zheng, J., Qiu, Y., Tabassum, T., Jang, J.H., Abu-Omar, M., Scott, S.L., Suh, S. (2020). Degradation Rates of Plastics in the Environment, *ACS Sustainable Chemistry & Engineering*, 8 (9), 3494–3511. DOI: 10.1021/acssuschemeng.9b06635

[5] Thompson, R.C., Moore, C.J., vom Saal, F.S., Swan, S.H. (2009). Plastics, the environment and human health: current consensus and future trends. *Philos. Trans. R. Soc. Lond. B. Biol. Sci*. 364 (1526), 2153-2166. DOI: 10.1098/rstb.2009.0053

[6] Briffa, J., Sinagra, E., Blundell, R. (2020). Heavy metal pollution in the environment and their toxicological effects on humans, *Heliyon*, 6 (9), e04691. DOI: 10.1016/j.heliyon.2020.e04691

[7] Hahladakis, J.N., Velis, C.A., Weber, R., Iacovidou, E., Purnell, P. (2018). An overview of chemical additives present in plastics: Migration, release, fate and environmental impact during their use, disposal and recycling, *Journal of Hazardous Materials*, 344, 179-199. DOI: 10.1016/j.jhazmat.2017.10.014

[8] Gómez-Sanabria, A., Kiesewetter, G., Klimont, Z., Schoepp, W., Haberl, H. (2022). Potential for future reductions of global GHG and air pollutants from circular waste management systems. *Nature Communications*. 13, 106. DOI: 10.1038/s41467-021-27624-7

[9] Sharma, S., Bhattacharya, A. (2017). Drinking water contamination and treatment techniques. *Appl. Water Sci.* 7, 1043–1067. DOI: 10.1007/s13201-016-0455-7

[10] Jury, W.A., Vaux, H. Jr. (2005). The role of science in solving the world's emerging water problems, *PNAS*, 102 (44), 15715–15720, DOI: 10.1073/pnas.0506467102

[11] Hunter, P.R., MacDonald, A.M., Carter, R.C. (2010). Water Supply and Health. *PLoS Medicine*, 7(11), e1000361. DOI: 10.1371/journal.pmed.1000361

[12] Howitt, P., Darzi, A., Yang, G.Z., Ashrafian, H., Atun, R., Barlow, J., Blakemore, A., Bull, A.M., Car, J., Conteh, L., Cooke, G.S., *et al.* (2012). Technologies for global health. *The Lancet Commissions*. 380 (9840), 507-535. DOI: 10.1016/S0140-6736(12)61127-1

[13] Boretti, A., Rosa, L. (2019). Reassessing the projections of the World Water Development Report. *npj Clean Water*, 2, 15. DOI: 10.1038/s41545-019-0039-9

[14] Dolan, F., Lamontagne, J., Link, R., Hejazi, M., Reed, P., Edmonds, J. (2021). Evaluating the economic impact of water scarcity in a changing world. *Nature Communications*, 12, 1915. DOI: 10.1038/s41467-021-22194-0

[15] Saravan, R.S, Muthukumaran, M., Mubashera, M., Abinaya, M., Prasath, P.V., Parthiban, R., Mohammad, F., Oh, W.C., Sagadevan, S. (2020). Evaluation of the photocatalytic efficiency of cobalt oxide nanoparticles towards the degradation of crystal violet and methylene violet dyes. *Optik - International Journal for Light and Electron Optics*, 207, 164428. DOI: 10.1016/j.ijleo.2020.164428

[16] Priya, R., Stanly, S., Dhanalekshmi, S.B., Mohammad, F., Al-Lohedan, H.A., Oh, W.C., Sagadevan, S. (2020). Comparative studies of crystal violet dye removal between semiconductor nanoparticles and natural adsorbents. *Optik - International Journal for Light and Electron Optics*, 206, 164281. DOI: 10.1016/j.ijleo.2020.164281

[17] Priya, R., Stanly, S., Kavitharani, K., Mohammad, F., Sagadevan, S. (2020). Highly effective photocatalytic degradation of methylene blue using PrO_2-MgO nanocomposites under UV light. *Optik - International Journal for Light and Electron Optics*, 206, 164281. DOI: 10.1016/j.ijleo.2020.164318

[18] Mathialagan, A., Manavalan, M., Venkatachalam, K., Mohammad, F., Oh, W.C., Sagadevan, S. (2020). Fabrication and physicochemical characterization of g-C3N4/ZnO composite with enhanced photocatalytic activity under visible light. *Optical Materials*, 100, 109643. DOI: 10.1016/j.optmat.2019.109643

[19] Fatimah, I., Ardianti, S., Sahroni, I., Purwiandono, G., Sagadevan, S., Doong, R.-A. (2021). Visible light sensitized porous clay heterostructure photocatalyst of zinc-silica modified montmorillonite by using tris (2,2′-bipyridyl) dichlororuthenium. *Applied Clay Science*, 204, 106023. DOI: 10.1016/j.clay.2021.106023

[20] Fatimah, I., Fadillah, G., Sahroni, I., Kamari, A., Sagadevan, S., Dong, R.-A. (2021). Nanoflower-like composites of ZnO/SiO_2 Synthesized using Bamboo Leaves Ash as Reusable Photocatalyst. *Arabian Journal of Chemistry*, 14, 3, 102973. DOI: 10.1016/j.arabjc.2020.102973

[21] Christy, A.J., Sagadevan, S., Nehru, L.C. (2021). Enhanced antibacterial and photocatalytic activities of nickel oxide nanostructures. *Optik*, 237, 166731. DOI: 10.1016/j.ijleo.2021.166731

[22] Hosny, N.M. (2011). Synthesis, characterization and optical band gap of NiO nanoparticles derived from anthranilic acid precursors via a thermal decomposition route. *Polyhedron*, 30, 470–476. DOI: 10.1016/j.poly.2010.11.020.

[23] D'Amario, L., Föhlinger, J., Boschloo, G., Hammarström, L. (2018). Unveiling hole trapping and surface dynamics of NiO nanoparticles. *Chemical science*, 9, 223–230. DOI: 10.1039/C7SC03442C

[24] Rath, M.K., Acharya, S.K., Kim, B.H., Lee, K.T., Ahn, B.G. (2011). Photoluminescence properties of sesquioxide doped ceria synthesized by modified sol–gel route. *Materials Letters*, 65(6), 955–958. DOI: 10.1016/j.matlet.2011.01.004

[25] Nguyen, K., Hoa, N.D., Hung, C.M., Le, D.T.T., Van Duy, N., Van Hieu, N. (2018). A comparative study on the electrochemical properties of nanoporous nickel oxide nanowires and nanosheets prepared by a hydrothermal method. *RSC Advances*, 8, 19449–19455. DOI: 10.1039/C8RA02862A.

[26] Zhang, X., Zhang, D., Ni, X., Song, J., Zhen, H. (2008). Synthesis and electrochemical properties of different sizes of the CuO particles, *Journal of Nanoparticle Research,* 10, 839–844. DOI: 10.1007/s11051-007-9320-9

[27] Allahyar, S., Taheri, M., Abharya, A., Mohammadi, K. (2017). Simple new synthesis of nickel oxide (NiO) in water using microwave irradiation. *Journal of Materials Science: Materials in Electronics*, 28, 2846–2851. DOI: 10.1007/s10854-016-5868-4

[28] Vidyasagar, C.C., Naik, Y.A., Venkatesha, T.G., Viswanatha, R. (2012). Solid-State Synthesis and Effect of Temperature on Optical Properties of CuO Nanoparticles. *Nano-Micro Letters*, 4(2), 73–77. DOI: 10.1016/j.powtec.2011.08.025

[29] Kumar, R.V., Diamant, Y., Gedanken, A. (2020). Sonochemical Synthesis and Characterization of Nanometer-Size Transition Metal Oxides from Metal Acetates. *Chemistry of Materials*, 12(8), 2301–2305. DOI: 10.1021/cm000166z

[30] Fazlali, F., Mahjoub, A.R., Abazari, R. (2015). A new route for synthesis of spherical NiO nanoparticles via emulsion nano-reactors with enhanced photocatalytic activity. *Solid State Sciences*, 48, 263–269. DOI: 10.1016/j.solidstatesciences.2015.08.022

[31] Miri, A., Mahabbati, F., Najafidoust, A., Miri, M.J., Sarani, M. (2022). Nickel oxide nanoparticles: biosynthesized, characterization and photocatalytic application in degradation of methylene blue dye. *Inorganic and Nano-Metal Chemistry*, 52, 122–131. DOI: 10.1080/24701556.2020.1862226

[32] Yáñez-Vilar, S., Sánchez-Andújar, M., Gómez-Aguirre, C., Mira, J., Señarís-Rodríguez, M.A., Castro-García, S. (2009). A simple solvothermal synthesis of MFe2O4 (M=Mn, Co and Ni) nanoparticles. *Journal of Solid-State Chemistry*, 182, 2685–2690. DOI: 10.1016/j.jssc.2009.07.028

[33] Revellame, E.D., Fortela, D.L., Sharp, W., Hernandez, R., Zappi, M.E. (2020). Adsorption kinetic modeling using pseudo-first order and pseudo-second order rate laws: A review. *Cleaner Engineering and Technology*, 1, 100032. DOI: 10.1016/j.clet.2020.100032

[34] Weldegebrieal, G.K. (2020). Synthesis method, antibacterial and photocatalytic activity of ZnO nanoparticles for azo dyes in wastewater treatment: A review. *Inorganic Chemistry Communication*, 120, 108140. DOI: 10.1016/j.inoche.2020.108140

[35] Weldegebrieal, G.K., Dube, H.H., Sibhatu, A.K. (2021). Photocatalytic activity of CdO/ZnO nanocomposite for methylene blue dye and parameters optimisation using response surface methodology. *International Journal of Environmental Analytical Chemistry*, 1–23. DOI: 10.1080/03067319.2021.1949589